Chemical Engineering Journal 377 (2019) 120123

Contents lists available at ScienceDirect

Chemical Engineering Journal

journal homepage: www.elsevier.com/locate/cej

Investigation of pressure drop in 3D replicated open-cell foams: Coupling CFD with experimental data on additively manufactured foams

Mauro Bracconi[a,b], Matteo Ambrosetti[a], Obinna Okafor[c], Victor Sans[c], Xun Zhang[d], Xiaoxia Ou[b], Claudio Pereira Da Fonte[b], Xiaolei Fan[b,*], Matteo Maestri[a], Gianpiero Groppi[a], Enrico Tronconi[a,*]

[a] Laboratory of Catalysis and Catalytic Processes – Dipartimento di Energia, Politecnico di Milano, Via La Masa 34, 20156 Milano, Italy
[b] School of Chemical Engineering and Analytical Science, The University of Manchester, Manchester M13 9PL, United Kingdom
[c] Faculty of Engineering, University of Nottingham, University Park, Nottingham NG7 2RD, United Kingdom
[d] Henry Moseley X-ray Imaging Facility, The Henry Royce Institute, School of Materials, The University of Manchester, Manchester M13 9PL, United Kingdom

HIGHLIGHTS

- Additive manufacturing of virtually-generated foams.
- Combined experimental and CFD study of the pressure drop through foams.
- Comprehensive assessment of pressure drop versus foam geometrical properties.
- New pressure drop correlations proposed for open-cell foams.

GRAPHICAL ABSTRACT

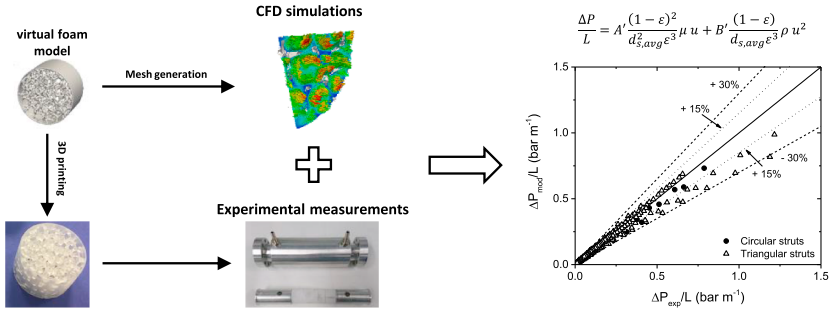

ARTICLE INFO

Keywords:
Open-cell foams
Virtual reconstruction
CFD
Additive manufacturing
Pressure drop

ABSTRACT

Open-cell foams as structured catalyst supports are promising candidates for the design of high throughput catalytic processes. In this contribution, we employ a coupled numerical and experimental approach to assess the pressure losses in foams. Large discrepancies between experimental results and predictions by empirical/analytical correlations are present in the literature, mainly due to the structural differences between adopted models and real foams. To exclude such structural differences, we explore virtually-generated foam models and their 3D printed replicas for a combined CFD and experimental study of fluid dynamics in foams. In particular, we focus our analysis on the low Reynolds number regime (Re $<$ 50), where deviations between the existing correlation and experimental data are more pronounced. We find a very good agreement between CFD simulations and experimental measurements in evaluating the pressure drop of gas flows across foams. The effect of porosity, cell sizes and strut shape are studied, leading to the derivation of an engineering correlation for the pressure drop in open-cell foams. Subsequently, the derived correlation is used to evaluate the trade-off between the external transport rate and the pressure drop, which is a pivotal aspect in most environmental catalytic processes: results show that open-cell foams can outperform honeycomb monoliths in the range of low Reynolds numbers.

* Corresponding authors.
E-mail addresses: xiaolei.fan@manchester.ac.uk (X. Fan), enrico.tronconi@polimi.it (E. Tronconi).

https://doi.org/10.1016/j.cej.2018.10.060

Available online 09 October 2018

Nomenclature

Latin letters

D_e	external diameter [m]
D_i	internal diameter [m]
H	sample height [m]
m	mass [kg]
L_{car}	characteristic length [m]
u	velocity [m/s]
ΔP	pressure drops [Pa/m]
K	Darcian permeability
L	Length [m]
S_v	specific surface area [m^{-1}]
A	viscous coefficient
B	inertial coefficient
A'_{pb}	Ergun viscous coefficient
B'_{pb}	Ergun inertial coefficient
d_p	sphere diameter [m]
$d_{s,avg}$	average strut diameter [m]
d_c	cell diameter [m]
	foam viscous coefficient
B'	foam inertial coefficient

Greek letters

ε_H	hydraulic void fraction [–]
ε_T	total void fraction [–]
ρ	density [kg/m^3]
μ	fluid viscosity [Pa s]
Γ	non-Darcian permeability

Subscripts

foam	related to the foam
strut	related to the strut material
solid	related to the foam solid material
EtOH	ethanol
cylinder	related to the cylinder
sample	related to the foam sample
skin	related to the external skin

Superscripts

air	air
EtOH	ethanol

Dimensionless numbers

$Re_{d_{s,avg}} = \frac{\rho u d_{s,avg}}{\mu}$ Reynolds number

1. Introduction

Open-cell foams are considered attractive structured catalyst supports for the intensification of catalytic processes limited by the external transport, such as automotive after-treatment systems [1], and environmental/chemical catalysis applications like partial oxidations [2], catalytic oxidation of methane [3], CO and methanol [4,5], methanol-to-propylene (MTP) reactions [6–8]. In addition, the improved mass transfer of foams also enables their applications in the context of chemical separations [9] and liquid phase reactions [10]. They are reticulated interconnected solid matrices, in which repeated open-cells are composed of solid struts and permeable open windows. Open-cell foams possess large surface area to volume ratio (or specific surface area, *e.g.* 2000 m^{-1}), promoting high mass and heat gas-to-solid transfer rates [11], and large void fractions (> 70%), resulting in low pressure drops [11]. In this view, open-cell foams are acknowledged as a promising solution for processes limited by the external mass transport where the reduced pressure drop are pivotal for the optimal operation of the system [11].

The pressure drops in open-cell foams have been well researched on an experimental standpoint based on two different approaches. On one hand, the experimental data have been modeled according to the hypothesis that the foam structure behaves like an ensemble of submerged object in cross flow. Giani et al. [11] performed an experimental investigation of pressure drops in different metallic foams with high porosity (> 92% and 10–40 pore per inch) and proposed a correlation in analogy to tube banks. Gancarczyk et al. [12] tried to correlate the pressure drops using a friction factor evaluated for the flow around the strut. The authors identified the flow around spheres with the size of node diameters as a good estimate for the pressure drops in open cell foams without reporting a theoretical explanation of this result. On the other hand, several authors tried to correlate pressure drops data by means of a Ergun-like equation [13–20]. Many characteristic lengths have been proposed (*e.g.* pore diameter, strut diameter and hydraulic diameter) and different numerical coefficients for viscous and inertial term as well. Despite this, the adequacy of the correlation is usually confined to a narrow range of geometrical properties or flow regimes, without obtaining an overall description of the different structures. Moreover, the choice of characteristic length introduces peculiar dependencies of the inertial and viscous coefficients on the morphological properties of foams usually based on empirical assumptions rather than on theoretical derivations. Among these correlations, the ones proposed by Dietrich et al. [18] and Inayat et al. [19] have been validated against the widest set of available literature data and are considered the most adequate estimates for pressure drops in open cell foams. In particular, Inayat et al. [19] developed a theoretically grounded model for the prediction of pressure drops in open cell foams accounting for the effect of the different morphological properties of foams assuming the hydraulic diameter as characteristic length and proposing a dependence of the Ergun coefficient from the tortuosity.

Pressure drops in open-cell foams have also been investigated by means of numerical simulations based on Computational Fluid Dynamics (CFD), which has been proven as a powerful tool for the estimation of pressure drops in porous media, exemplified by relevant simulation works using idealized unit cells [21,22], tomographic reconstructed foam models [23] and virtually generated foam models [24,25]. The simulations carried out on ordered arrays of unit cells have been demonstrated to be unrepresentative of the real behavior due to the lack of randomness characteristic of these structure [26].

In spite of the extensive research conducted for proposing pressure drops correlations in foams, severe deviations between empirical/analytical correlations and experimental data up to ± 100% are present, as highlighted by Edouard et al. [16]. In particular, the description of the low Reynolds regime shows the largest deviations between experimental data and model predictions, as recently pointed out by Kumar and Topin in their review on the state-of-the-art of pressure drop correlations [27]. The pressure drop in the low Reynolds regime, which shows the most favorable tradeoff between external mass transfer and pressure drops [11], is usually underestimated by the state-of-the-art correlations [19].

The deviations between the experimental data and the predictions of the correlations can be ascribed to the discrepancies between the idealized/simplified models and the real structures. Open-cell foams possess a complex and stochastic structure which can hardly be

adequately described by repetitive arrays of simple and ordered unit cells. Moreover, the existing literature correlations are usually derived at high Reynolds number and, hence, the predictions at low flow rates are usually an extrapolation of data obtained in different operating conditions, making them inaccurate for the description of the low Re region. Thus, we carried out a detailed investigation of the low Re regime in order to extend the current correlations, which are relatively accurate in the high Re range [19]. To achieve this purpose, in this contribution we exploit structures generated according to a virtual reconstruction procedure [25] to exclude the effect of uncertainties in the description of the foam geometry, being the virtual samples totally and accurately defined and characterized, and to investigate the interactions between foams and fluid flow. The virtual reconstruction has been proved to show analogous overall geometrical properties, *i.e.* specific surface area, porosity, and the same flow behavior of the real foam structures [25]. Thus, the reconstruction is able to provide virtual foam samples which can be employed for the accurate investigation of the momentum transfer in these structures. The procedure enables a two-fold investigation of open-cell foams. On one hand, the virtual foams can be numerically analyzed using CFD, providing a deep insight into the flow field established in open-cell foams and allowing for the estimation of the pressure gradient along the structure. On the other hand, the additive manufacturing (*i.e.* 3D printing) generates real samples (resin as the base material) based on the virtually reconstructed models (with the identical characteristics defined by the virtual models), enabling the direct experimental validation of the CFD simulated results. The significance of this approach lies in the removal of the uncertainties between the numerical simulations and the experiments, thus filling the gap between the theoretical model and the real samples.

In this work, we propose an original approach for the combined numerical/experimental investigation of the transport property using the identical virtual reconstructed and additive manufactured foams to understand the effect of the geometrical properties of porosity, cell size and strut shape on the pressure drop in open-cell foams. This approach enables us to derive an Ergun-like correlation for the accurate description of the pressure drops across foams (with the assumption of the average strut size as characteristic length), which correctly accounts for their effects. As a whole, the conclusions of this work improve the current state-of-the-art extending the accuracy of pressure drop correlations also to the low Reynolds regime.

2. Methods and models

2.1. Virtual foam reconstruction

Computational fluid dynamics (CFD) simulations are carried out on a virtual reconstruction of open-cell foams previously proposed, which fully retains the geometrical and fluid-dynamic properties of open-cell foams [25]. The reconstruction procedure relies on a few pieces of easily-accessible geometrical information, *e.g.* cell diameter, strut cross-sectional shape and porosity. The foam skeletal structure is generated by means of a Voronoi-tessellation which partitions the tridimensional space around an ensemble of points, generating a space-filling collection of polyhedrons with no space or gaps and is acknowledged as a suitable guess for the foam skeleton [28]. The initial seeds required by the algorithm are obtained by means of a random packing of spheres with the required cell diameter. The exact description of the strut and node geometry is crucial to accurately describe the complex foam microstructure. Thus, dedicated models for the description of the struts and nodes are proposed [29]. Three different porosities are considered to investigate the effect on the pressure drop and three different cell sizes with dimensions compatible with the resolution of the 3D printing ($> 200\,\mu m$) are selected as well.

A parabolic profile is assumed for the variation of the strut diameter along the ligaments axis. Different shapes of the strut cross-sectional, *i.e.* circular or triangular, are accounted by changing the ligament shape. Dedicated node geometry has been proposed to properly account for the region where the struts join. The virtually generated foams show a good agreement with experimental measurements for both the geometrical property and pressure drop. More details on the procedure can be found elsewhere [25].

Table 1
Geometrical features of the virtually-generated open-cell foams exploited for CFD numerical simulations and 3D printing.

Foam sample	d_c [mm]	ε [–]	S_v [m^{-1}]	$d_{s,avg}$ [mm]
A[a]	3.00	0.70	985	0.85
B[a]	4.00	0.70	738	1.13
C[a]	5.00	0.70	591	1.41
D[a]	3.00	0.80	935	0.62
E[a]	4.00	0.80	701	0.82
F[a]	5.00	0.80	561	1.03
G[a]	3.00	0.90	763	0.38
H[a]	4.00	0.90	572	0.50
I[a]	5.00	0.90	458	0.63
J[b]	4.00	0.90	722	0.66

[a] Strut with circular cross-sections.
[b] Strut with triangular cross-sections.

Ten foam structures with the variation in the cell size, porosity and strut shape have been generated. The geometrical properties of the foam structures are reported in Table 1. The effect of the strut cross-sectional shape has been analyzed by comparing virtual samples generated using the same porosity and cell size but different ligament shape. The structures are generated as disks of 25.8 mm of diameter and 20 mm length, dimensions compatible with the 3D printer. Moreover, an external surface with a thickness of 0.5 mm is added to improve the quality of the printed samples in terms of structural integrity. The CAD models are shown in Fig. 1.

2.2. Computational domains for CFD simulation

The computational domain for CFD simulation is generated from the surface file resulting from the foam reconstruction procedure, by means of the snappyHexMesh utility of the OpenFOAM framework [30]. This utility starts from a uniform background mesh, then refines the region of the computational domain around the surface using the cut-cell method, and finally projects the mesh vertices on the surface. Thus, a body-fitted mesh being able to catch all the details of the original geometry is obtained. The computational domain consists of a quarter of the foam disk, whose diameter and length are equal to 26.8 and 20.0 mm, respectively. Thus, the performance of the system can be predicted by the simulation of a single layer of the stack. A quarter of the disk is simulated due to the symmetry of the system. The foam geometrical property is evaluated on the quarter and compared to that of the full disk to assess the quality of the approximation. A negligible difference in the porosity and specific surface area is obtained since the variations are below 0.5% and 2%, respectively. An analogous approach has been successfully used by Razza et al. [31] in the context of conjugate heat transfer in open-cell foams. Symmetry boundary conditions are imposed in the coordinate transversal to the fluid flow for all variables. No slip and Neumann boundary conditions are imposed on the surface of the foam and on the tube wall for the velocity field and pressure, respectively. Atmospheric pressure is imposed at the outlet boundary, while a Neumann boundary condition for the inlet is considered. To mimic the behavior of the stack of foam disks, cyclic boundary conditions are imposed for velocity in the stream-wise direction, according to the procedure reported by Bracconi et al. [25].

Mesh convergence analysis has been carried out to obtain a solution independent from the computational domain. Several background meshes have been tested with three levels of refinement around to the foam surface. A dense mesh around the surface is required to properly describe the momentum gradients around the surface and the surface

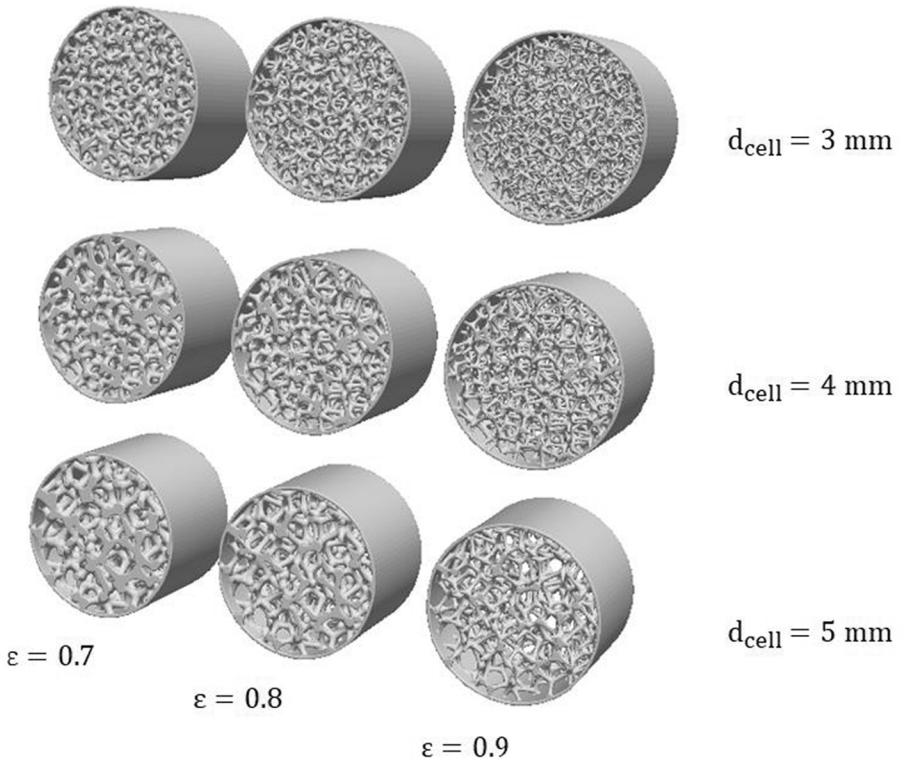

Fig. 1. Virtually-generated models with different porosities (0.7, 0.8, 0.9), different cell sizes (3 mm, 4 mm, 5 mm) and circular struts.

friction. An influence of the mesh on the target quantity, *i.e.* pressure drop, below 2% is reached with a ratio between the cell diameter and grid size of the background mesh equal to 20. The mesh is carefully generated to obtain high-quality grids with low non-orthogonality and skewness values. The simulation is performed with simpleFoam, a numerical solver of the OpenFOAM framework [30], developed for incompressible laminar and turbulent flows. Ambient air at 298 K (density = 1.18 kg m^{-3}; dynamic viscosity = 1.86×10^{-5} Pa s) is used as working fluid. The simulations are carried out using a laminar model, according to literature results [32], as well as to our previous findings [25]. A second order scheme (linear upwind) is adopted for the convective terms, whereas a second-order scheme is used for the Laplacian terms.

2.3. Additive manufacturing (3D printing) of foam replica

The foam samples are generated by means of stereolithography (SLA) [33], an additive manufacturing technique being able to produce solid models in a layer by layer fashion using photopolymerization. Stereolithography is a common Vat Polymerisation technique, one of the seven American Section of the International Association for Testing Materials (ASTM) categories of additive manufacturing. In this work, we employ the Formlabs Form 2 printer to build the samples in an off-the-shelf proprietary Clear (RS-F2-GPCL-02) acrylic resin. The printer is set to work with the high level of resolution for the layer thickness (25 μm), introducing a constraint on the minimum dimension of struts since the ligaments should be > 3 layers to enable an accurate manufacturing of the elements.

Fig. 2 shows the example of 3D printed foam samples which consist of both the internal foam and the external skin. The external skin has been proved to strongly improve the structural integrity of the printed samples, particularly for foams with small cell sizes and strut diameters (d_c < 4 mm), which require the presence of the external skin to avoid structural collapse during the printing. Additionally, the external skin also ensures a tight fit of the samples in the test reactor, avoiding the possible wall effect.

2.4. Experimental rig

The pressure drop across the 3D printed samples is measured for velocities in the range of 0.1–1 m s^{-1}. The foam bed with four equal samples is used in each test to ensure an adequate pressure loss to be measured. A specially designed aluminum tube (ID = 26.6 mm) is used for the measurement, as shown in Fig. 3. The additively manufactured samples are polished with sandpaper and then wrapped with Teflon tape to avoid wall effect. Two spacers are loaded on both ends of the reactor to ensure the precise positioning and tight contact between foams. Two pressure ports are introduced (as shown in Fig. 3) to enable the measurement of the pressure located respectively 4 cm before and after the foam bed. Additional pressure drops induced by the setup are expected to be negligible.

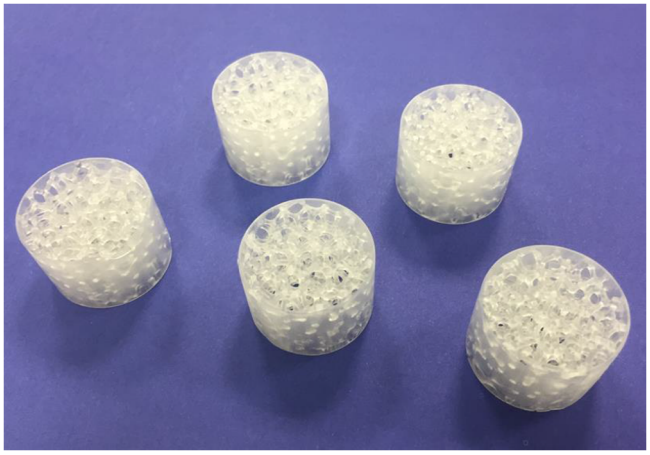

Fig. 2. Examples of 3D printed samples for the foam with the cell size of *ca.* 4 mm and porosity of 0.8.

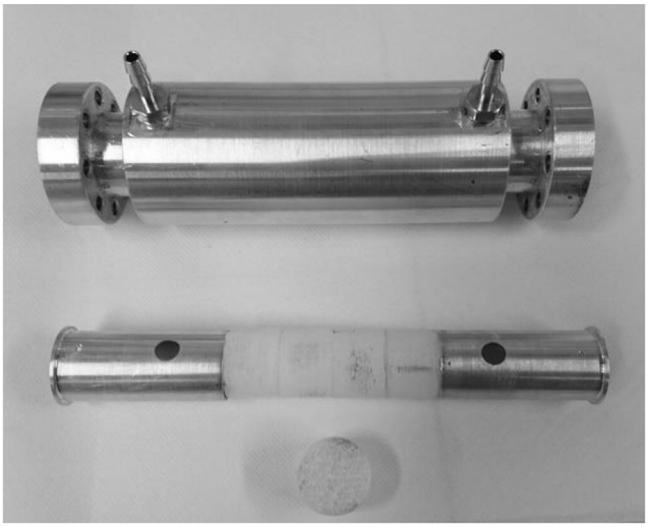

Fig. 3. Experimental reactor along with the foam bed consisting of a stack of four foams.

Pressure drop is measured with a differential manometer TM 265–1 (Techmark) with the range of 0–100 Pa (sensibility = 0.01 Pa, precision = 0.1 Pa). To avoid over-pressurizing the lines, the exit of the reactor is open to the ambient. The gas flow rate was regulated with a mass-flow controller (Brooks 5851 with a precision of ± 0.04 standard liter per minute (SLM)). The mass-flow controller is calibrated with a bubble flow meter and then operated in the range 2–30 SLM.

2.5. Gravimetric analysis

The additive manufactured foams are characterized to assess the consistency of their geometrical properties in reference to the virtual foams. In particular, the analysis is focused on the hydraulic porosity, *i.e.* the porosity accessible to the fluid flow, which is an important parameter in the description of the transport property. The porosity of open cellular structures is commonly described by the total porosity ε_T and hydraulic porosity ε_H [34], defined as

$$\varepsilon_T = 1 - \frac{\rho_{foam}}{\rho_{solid}} \tag{1}$$

$$\varepsilon_H = 1 - \frac{\rho_{foam}}{\rho_{strut}} \tag{2}$$

where ρ_{foam}, ρ_{strut} and ρ_{solid} are the foam density, strut density and density of the solid material, respectively.

The two porosities may differ due to the eventual presence of inner cavities in the struts. The foam density is estimated by dividing the weight of the foam by its total measured volume. Since the printed foams have an external skin, the density is evaluated as:

$$\rho_{foam} = \frac{m_{foam}^{air} - V_{skin}\rho_{strut}}{V_{sample} - V_{skin}} \tag{3}$$

$$V_{skin} = \frac{\pi}{4}(D_e^2 - D_i^2)H \tag{4}$$

$$V_{sample} = \frac{\pi}{4}D_e^2 H \tag{5}$$

where m_{foam}^{air} is the mass of the foam weighted in air, V_{sample} is the overall sample volume, V_{skin} is the mass of the external skin, D_e and D_i are the external and internal diameter of the sample, respectively, and H is the length of the sample. The arithmetic average values of the diameter and height were measured with a Vernier caliper at different axial and radial positions of the additive manufactured foams.

The density of the strut is evaluated using a standard pycnometry method, according to Eq (6), based on the measurement of the buoyancy of the samples in ethanol (using the Sartorius YDK 01 density determination kit in reference to a printed full cylinder of the strut material).

$$\rho_{strut} = \frac{m_{cylinder}^{air}\rho_{EtOH}}{m_{cylinder}^{air} - m_{cylinder}^{EtOH}} \tag{6}$$

where $m_{cylinder}^{air}$ is the mass of cylinder in air, $m_{cylinder}^{EtOH}$ is the mass of cylinder in ethanol and ρ_{EtOH} is the density of ethanol. As expected, the 3D printer generates material without internal voids since the strut density is equal to the solid density. Thus, measurement of the total and hydraulic porosity returns the same value (*i.e.* $\varepsilon_T = \varepsilon_H = \varepsilon$).

2.6. Scanning electron microscopy (SEM) and micro-computed tomography (μCT)

SEM and μCT characterization are performed in order to compare the additive manufactured replica with the CAD model. SEM analysis of the 3D printed samples is performed using a FEI Quanta 200 ESEM machine in high voltage mode (8 kV) with a magnification of 60 × to assess the surface morphology. μCT scans are performed using a Nikon XTEK XTH 225 kV cabinet system. The sample is placed on a rotating holder irradiated by a cone beam of the X-ray source generated by a tungsten target with an accelerating voltage of 60 kV. X-ray images are recorded for a set of 3601 equally spaced rotational positions using a flat panel detector (3192 × 2296) and an acquisition time of 1 s. Sample E (see Table 1) has been scanned with a voxel size of 14 μm per pixel which is a good tradeoff between the accuracy and computational cost and enables the scan of each strut with > 50 voxels in the transversal direction. A set of raw 3D images has been postprocessed using Avizo 9.4 software to generate a tri-dimensional structure of the scanned sample. In doing so, each voxel is assigned to the fluid or solid phase by selecting a threshold grey value. Once each voxel is assigned, it is possible to extract the 3D reconstruction of the structure. The reconstructed virtual slices have a voxel size of 14 × 14 × 14 μm^3.

2.7. Pressure drops modeling

The pressure gradient across the foam can be expressed as a function of the geometrical and fluid properties and the fluid velocity (Eq. (7)).

$$\frac{\Delta P}{L} = f(L_{car}, \varepsilon, u, \rho, \mu) \tag{7}$$

where L_{car} is a characteristic length, ε is the porosity, u is the superficial velocity, ρ is the gas density, μ is the gas viscosity and L is the foam length. The modeling of pressure drop was carried out with the aim to derive a correlation of the pressure gradient in relation to the fluid velocity and geometrical parameters. In this view, the most common modeling approach follows the Darcy-Forchheimer equation (Eq. (8)), which has been extensively used in the literature to describe the pressure drops of packed beds, as well as porous media.

$$\frac{\Delta P}{L} = \frac{\mu}{\mathrm{K}}u + \frac{\rho}{\Gamma}u^2 \tag{8}$$

where K and Γ are the Darcian and non-Darcian permeabilities, respectively. These parameters are a function of the geometrical characteristics of the packing. Ergun and Orning [35] proposed a theoretical interpretation of the permeability in the context of packings made of spherical pellets, resulting in the Ergun equation, the state-of-the-art correlation for the evaluation of the pressure drop in packed beds. In particular, the Kozeny assumption [36] was applied, assuming that the granular bed is equivalent to an ensemble of parallel, equally sized channels. Therefore, the total internal surface and the free internal volume of the packing are equal to the total packing surface and to the void volume, respectively, of the packed bed. Under these assumptions, the pressure gradient in granular media assumes the expression as in

Eq. (9),

$$\frac{\Delta P}{L} = A\frac{S_v^2}{\varepsilon^3}\mu u + B\frac{S_v}{\varepsilon^3}\rho u^2 \tag{9}$$

where S_v is the specific surface area of the packing; and A and B are the Ergun constants for viscous and inertial terms.

By introducing the pellet diameter d_p, Eq. (9) appears in the most common form ($S_{v,pb} = 6(1-\varepsilon)/d_p$) of Eq. (10).

$$\frac{\Delta P}{L} = A_{pb}^{'}\frac{(1-\varepsilon)^2}{d_p^2\varepsilon^3}\mu u + B_{pb}^{'}\frac{(1-\varepsilon)}{d_p\varepsilon^3}\rho u^2 \tag{10}$$

The viscous and inertial coefficients were recovered from a regression on a broad set of experimental data and the values are 150 and 1.75, respectively. Macdonald et al. [37] estimated the coefficients on the basis of additional datasets and proposed 180 and 1.8 for the constants A and B. However, the empirical nature of the Ergun's coefficients hinders the direct application of the correlation to foam-like structures due to the evident difference between the porosity and other structural properties of foams and packed beds. Thus, dedicated numerical and experimental tests are carried out to obtain an Ergun-like equation applicable to foam structures.

3. Results and discussion

3.1. Geometrical characterization of the virtual and 3D printed foams

The comparison between the hydraulic porosity of the virtual (CAD) and 3D printed foams is shown in Fig. 4. The solid fraction of 3D printed samples is higher than that of CAD counterparts, with deviations < 5%. This is in line with the relevant findings on the periodic ordered cellular structures generated by additive manufacturing [38].

Based on the visual inspection, the additional material seems to be present close to the external skin of the 3D printed samples. This is due to the printing procedure, in which the samples were dipped in the resin, causing the additional resin trapped due to the capillary effects. The deviation is related to the porosity, *i.e.* the smaller the porosity, the larger the deviation, because a large number of struts in low porosity resin foams (which intersect the external skin and reduce the permeability) increase the amount of resin trapped close to the skin. To confirm this hypothesis, a μCT scan of Sample E was performed. The CT reconstruction of the virtual sample is presented in Fig. 5(a). The porosity of the CT reconstruction is evaluated by removing the external wall to compare the result with the experimental measurements by pycnometry. A good agreement was observed with deviations < 1% (*i.e.* μCT 0.785 *vs.* experimental 0.791), proving the adequacy of the threshold value. A direct comparison between a CAD file and a μCT reconstruction of the printed foam was carried out. In doing so, the CAD file (grey model) was superimposed on the μCT reconstruction (yellow model) to highlight the presence of deviations between the two surfaces. The internal region of the two shows insignificant deviations. Moreover, the local structure of the foam is accurately reproduced in the printed replica, confirmed by the absence of pore clogging or local irregulates. However, the region of the μCT sample near the external wall presents an accumulation of the solid material as shown in Fig. 5(b). The region at the bottom presents residuals from the SLA process which form an additional layer of solid material, as shown by the predominant yellow color. This analysis demonstrates that the deviation between the porosity of the CAD file and the one of the printed samples are confined in a layer close to the external wall. Hence, we assume that the deviation in porosity between the CAD file of the virtual reconstruction and the printed sample is insignificant in the comparative study of pressure drop of this work.

The morphology of a printed foam is investigated by SEM to analyze the presence of superficial irregularities or roughness. As depicted in Fig. 5(c and d), the printed foam manufactured by SLA shows a smooth surface without surface roughness. The manufacturing process consists of a layer-by-layer solidification of resin which is evident by SEM. However, the scale of layers is relatively smaller than that of the strut diameter, suggesting the insignificant deviation between the CAD model and the printed counterpart. Therefore, additional drag (and hence the pressure drop) is unlikely by the printed samples in experiments. In this view, numerical simulations are carried out using the CAD model without any modifications since they represented the real samples appropriately.

3.2. Effect of the cell size on the pressure drop

The effect of the cell size on the pressure drop is assessed by both CFD simulations of air flow through virtual foams and experimental measurements using 3D printed foams (Samples D, E and F in Table 1), in which the porosity (0.8) and strut shape (with circular cross-sections) of foams are kept constant. Fig. 6 shows the pressure drop as a function of the flow velocity, exhibiting its increasing trend with a decrease in the cell size at a constant porosity. This can be explained by the variation in the surface area to volume ratio of the samples, which is inversely proportional to the cell size, *i.e.* the smaller the cell size, the higher the surface area, and hence the higher the friction drag. Within the range low Reynolds number (< 50), the experimental data show a good agreement (average deviations of 8% with the maximum deviation of 12%) with the numerical simulations in this study as shown in Fig. 6(b). Conversely, in the literature [16,27], the deviations between the correlations and experimental data are usually large (> 50%).

3.3. Effect of the porosity on the pressure drop

The dependence of the pressure drop on the porosity of foams (Samples B, E and H) was investigated in the void fraction of 0.7–0.9, covering the typical porosity values of open-cell foams. The synthetic procedure to generate the structure allows for employing the same foam skeleton reaching the required porosity by changing the node and strut size. The cell size has been fixed as 4.0 mm and struts with the circular cross-section have been considered in the procedure, enabling the study of the sole effect of foam porosity on the pressure drop. The simulation results are presented in Fig. 7a, showing that, as expected, the pressure drop (*i*) is inversely proportional to the porosity and (*ii*) directly proportional to the fluid velocity (at 0–4 m s^{-1}, according to the typical Darcy-Forchheimer behavior). In the range of 10 < Re < 280

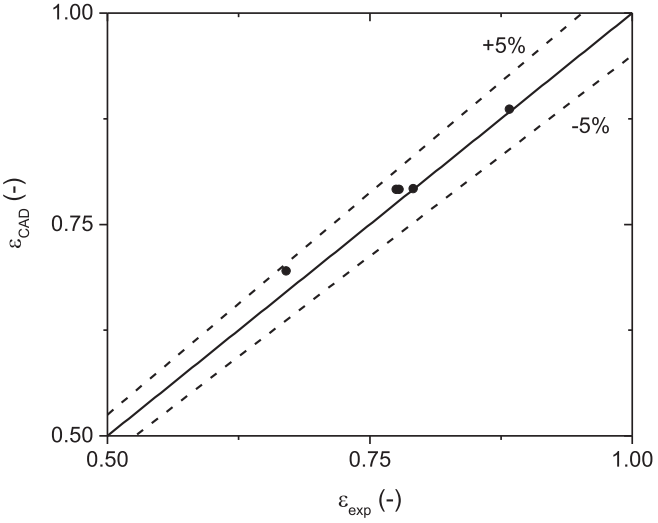

Fig. 4. Experimentally measured hydraulic porosity of 3D printed foams against the hydraulic porosity evaluated on the virtual foams.

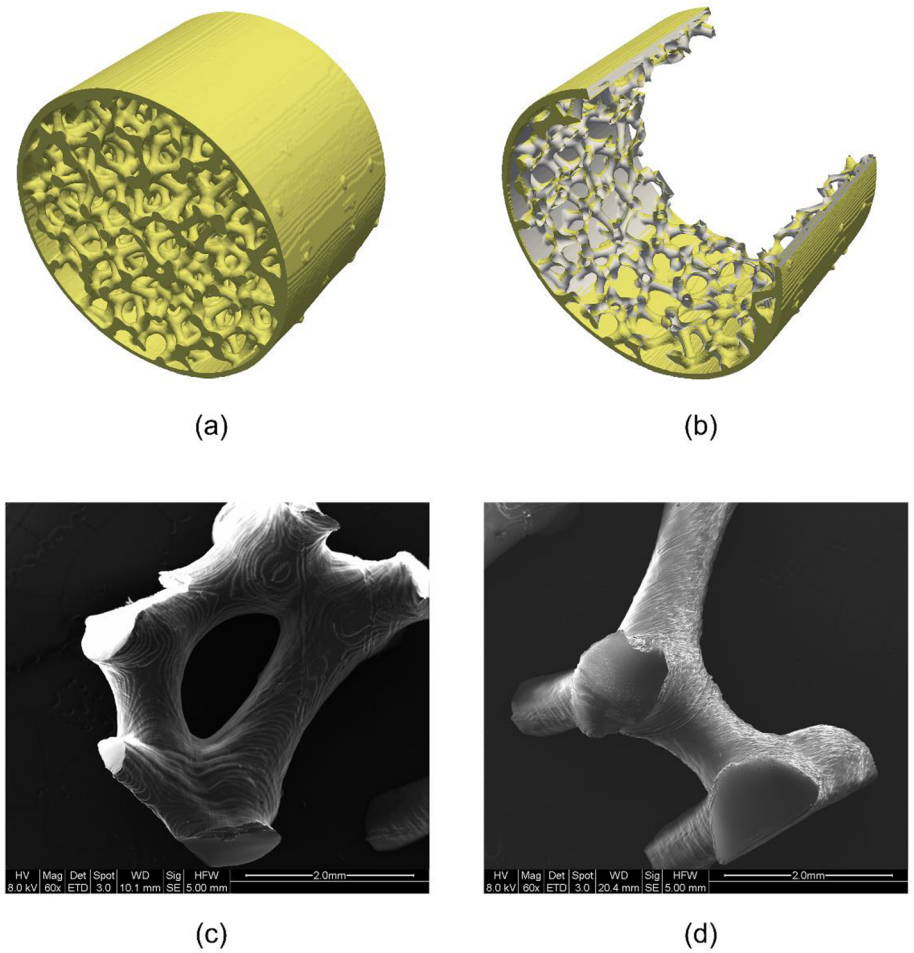

Fig. 5. μCT scan of an SLA printed Sample E (a) along with the comparison between the CAD (grey) and the tomographic reconstruction (yellow) of the region close to external wall (b). SEM micrographs of morphological details of an SLA printed foam (c and d). (For interpretation of the references to color in this figure legend, the reader is referred to the web version of this article.)

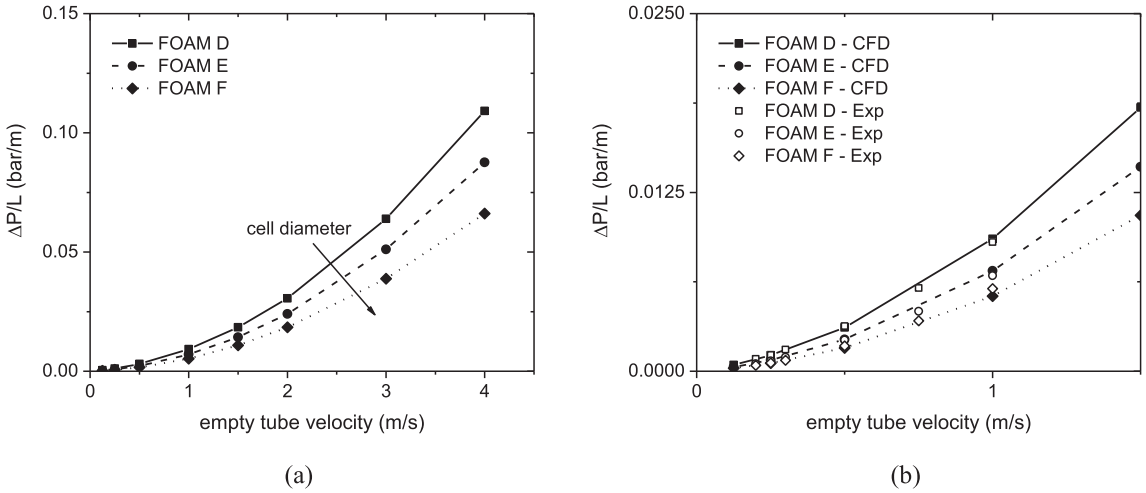

Fig. 6. Pressure drop as a function of the empty tube velocity for three different cell diameters (3 mm – solid line, 4 mm – dashed line, 5 mm – dotted line) and constant porosity of 0.8: (a) CFD simulations for velocity in the range of 0–4 m s^{-1} (full symbols) and (b) comparison with experimental data (open symbols) of 0–1 m s^{-1}.

(Fig. 7b), the relevant experimental data are superimposed to the numerical simulation, showing capability of the numerical method to describe the complex interaction between the fluid flow and foams.

3.4. Effect of the strut shape on the pressure drop

Two foam samples (Samples H and J in Table 1) with equal porosity and cell size, but different strut geometries (including the nodes), *i.e.* circular and triangular cross-sections, were investigated both

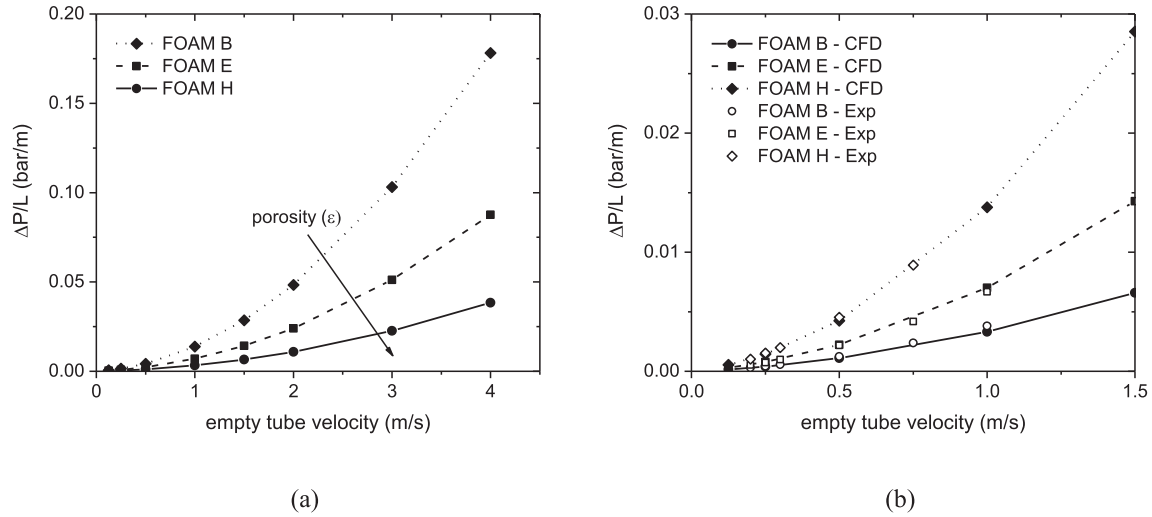

Fig. 7. Pressure drop as a function of the empty tube velocity for three different porosities (0.9 – solid line, 0.8 – dashed line, 0.7 – dotted line) and constant cell size equal to 4 mm: (a) CFD results for velocities in the range of 0–4 m s^{-1} (full symbols) and (b) comparison with experimental data (open symbols) in the range of 0–1 m s^{-1}.

experimentally and numerically to show the shape effect on the pressure drop (Fig. 8). The two foams were generated with the same initial seed of the Voronoi tessellation, the same porosity (0.9) and cell size (4 mm). CFD simulation of air flow through the two foams (Fig. 7) shows that the foam with the triangular struts causes the higher pressure drops of 15–20%, especially at high empty tube velocities (*i.e.* > 1.5 m s^{-1}), than the one with circular struts. This phenomenon can be mainly related to the difference in their large surface area to volume ratios, S_v (Table 1). The foam with the triangular struts presents a higher S_v than the counterpart with circular struts, leading to a higher drag coefficient. This finding emphasizes that the shape of struts in open-cell foams should be carefully accounted for the proper description of the pressure drop.

3.5. Revised pressure drop correlations for open-cell foams

We propose an Ergun-like equation for describing the pressure drop across the open-cell foam bed. By considering the Kozeny assumption [36] valid, also in the context of foams, Eq. (9) in its general form is still valid. Thus, the problem is related to the definition of (*i*) the model being able to evaluate the specific surface area and (*ii*) the characteristic length of foam packings. We tackled the first issue by adopting a fully-theoretically grounded geometrical model for the description of the geometrical property of open-cell foams which has been recently proposed by our group [29]. In terms of the characteristic length of foams, the hydraulic diameter [19,39], pore diameter [21] and cell diameter [32] were proposed for pressure drop correlations. In this work, we proposed the average strut diameter [40] as the characteristic length, which is evaluated according to the geometrical model proposed by Ambrosetti et al. [29].

As shown in Fig. 9, the specific surface area correlates well to the term of solid fraction and average strut size, which is the average diameter for circular struts and the average side length of the triangle for triangular cross-sectional shape, respectively. A quasi-linear relationship is obtained and deviations < 2% from a straight line were observed at the relatively low porosity ($\varepsilon < 0.75$). The relationship between the characteristic length and the specific surface area shows a functional form similar to the well-known relationship for packed beds. The proportionality coefficient assumes a value which is around 2.86 for circular struts and 4.85 for triangular struts, which are lower than the values for packed beds.

The specific surface area can be written in the form of Eq. (11).

$$S_v \cong k\frac{(1-\varepsilon)}{d_{s,avg}} \tag{11}$$

where k is the proportionality constant (2.85 and 4.86 for circular and triangular strut, respectively).

Thus, the pressure drop across the open-cell foam can be estimated according to Eq. (12).

$$\frac{\Delta P}{L} = A'\frac{(1-\varepsilon)^2}{d_{s,avg}^2\varepsilon^3}\mu u + B'\frac{(1-\varepsilon)}{d_{s,avg}\varepsilon^3}\rho u^2 \tag{12}$$

Eq. (12) can be conveniently rewritten in a dimensionless form as:

$$\frac{\Delta P d_{s,avg}^2}{L\mu u} = A'\frac{(1-\varepsilon)^2}{\varepsilon^3} + B'\frac{(1-\varepsilon)}{\varepsilon^3}Re_{d_{s,avg}} \tag{13}$$

where the Reynolds number is defined as:

$$Re_{d_{s,avg}} = \frac{\rho u d_{s,avg}}{\mu} \tag{14}$$

Fig. 10 presents the dimensionless pressure drop (Eq. (13)) as a function of the Reynolds number, showing generally a linear trend.

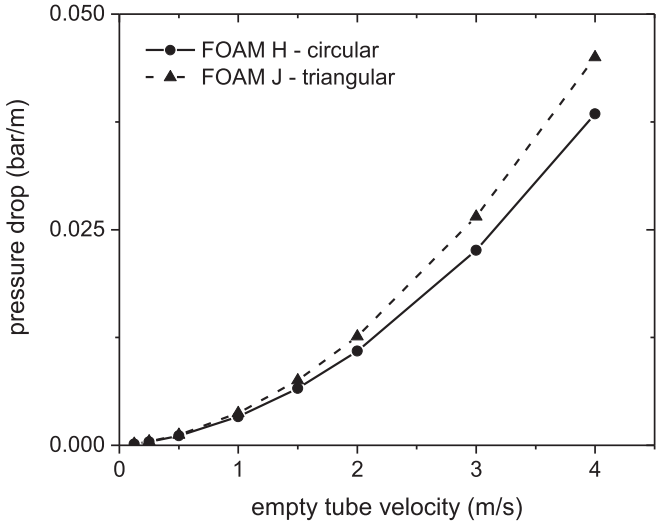

Fig. 8. Pressure drop as a function of the empty tube velocity for circular (solid line) and triangular (dashed line) for a foam with d_c = 4 mm and porosity equal to 0.9.

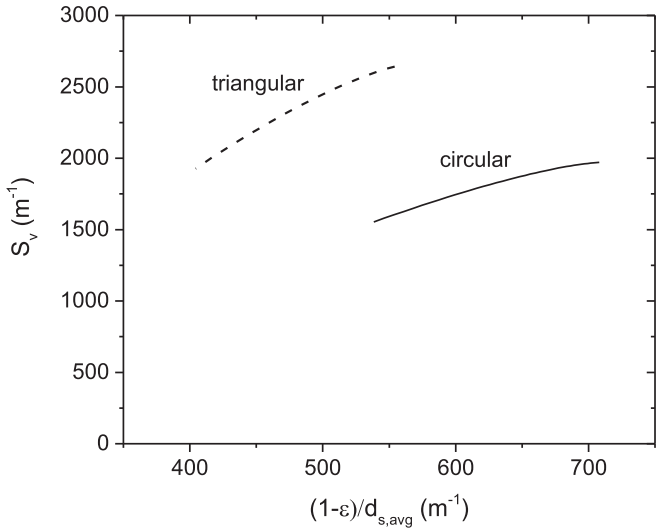

Fig. 9. Specific surface area for circular (solid line) and triangular (dashed line) strut with respect to the solid fraction and average strut diameter.

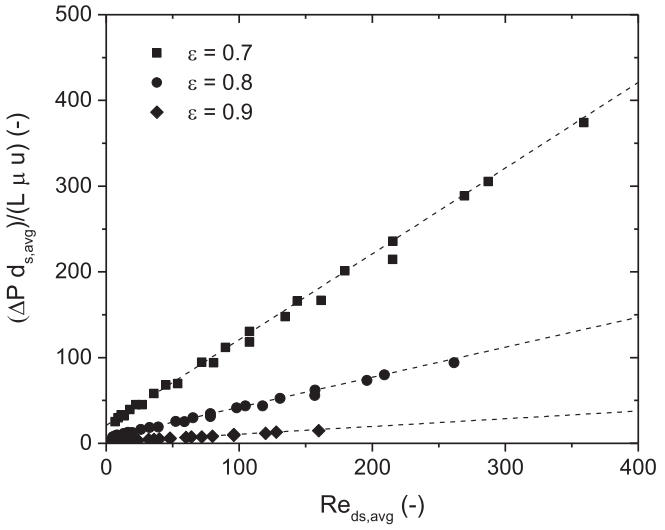

Fig. 10. Dimensionless pressure drop against Reynolds number for different porosity and cell sizes from CFD simulations.

Interestingly, the slope of linear fits changes according to the porosity of the foam. Moreover, the adoption of the average strut diameter is sufficient to account for the different cell sizes without requiring additional parameters. Thus, the A and B parameters of the Ergun-type equation mainly depend on the porosity.

According to Eq. (12), the pressure loss through foams consists of the viscous and inertial term, which are all functions of the porosity, *i.e.* the viscous energy loss $\propto (1-\varepsilon)^2/\varepsilon^3$ and the inertial energy loss $\propto (1-\varepsilon)/\varepsilon^3$. Based on the data in Fig. 10, the Ergun constants (A and B) as function of $(1-\varepsilon)^2/\varepsilon^3$ and $(1-\varepsilon)/\varepsilon^3$, respectively, are plotted in Fig. 11, showing the decreasing trend of A and B by increasing the porosity (ε) leading to lower pressure drops.

The numerical and experimental tests revealed that the viscous and inertial coefficients show the same functional dependence with respect to the porosity as the one theoretically proposed by Ergun for packed bed reactor [41].

The circular or triangular cross section of the strut influences the fluid flow around the foam solid matrix, resulting in higher pressure drop for the latter at the same fluid superficial velocity, as shown in Section 3.4. By a careful examination of the dimensionless pressure drop as the function of Re (Fig. 12), it highlights that two sets of coefficients should be considered for the proper description of the effect of strut shapes in correlations of Eq. (13), as already proposed by Inayat et al. [19].

It is worth emphasizing that the different strut-cross sectional shapes are accounted by the constants A' and B' without losing the functional dependence from pore densities and porosities.

Based on the simulation and experimental data from this study, the viscous and inertial constants (A' and B') of Eq. (12) are extracted by the regression analysis, as shown in Table 2. The constants for the foams with circular struts were estimated based on the data set of 102 (72 from the numerical simulations and 30 from the experimental tests). For the foams with triangular struts, the constants were derived from the one of circular struts, by considering the relationship between the specific surface area and average strut diameter for circular and triangular struts, because only one foam sample with triangular struts has been investigated. This approach was considered as meaningful because a quasi-linear relationship between the specific surface area and the solid fraction divided by the average strut diameter is valid for both strut shapes, according to the geometrical model by Ambrosetti et al. [29] (Fig. 9).

Fig. 13 shows a parity plot where the predictions by the correlation of Eq. (12) are compared to the CFD simulated and experimental

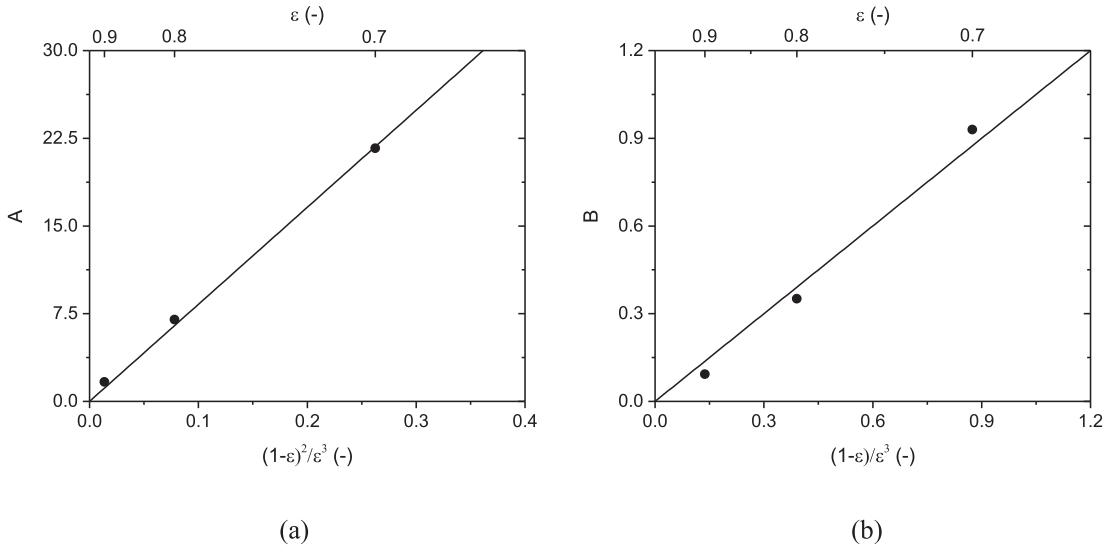

Fig. 11. Dependence of (a) the viscous and (b) inertial coeffects with respect to the void fraction.

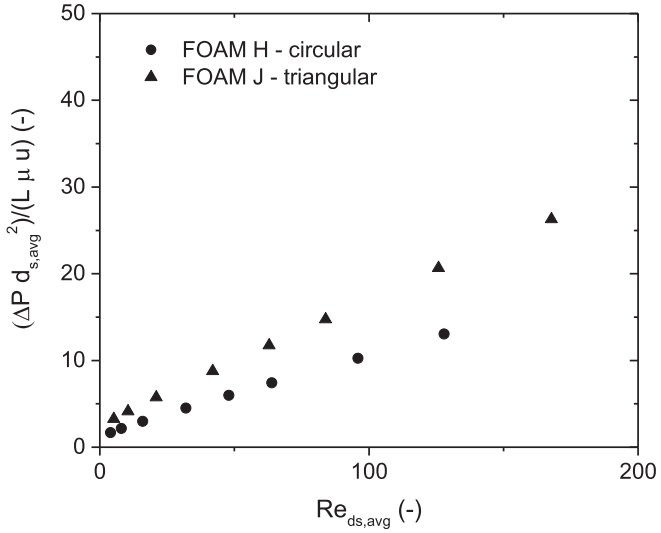

Fig. 12. Dimensionless pressure drop as a function of the Reynolds number for foam with cell size of 4 mm and porosity of 0.9 but different strut cross-sectional shape.

Table 2
Viscous and inertial constants for the proposed pressure drop correlation of open-cell foams.

A'_{circ}	92
B'_{circ}	0.71
A'_{triang}	266
B'_{triang}	1.20

results, showing a good agreement with deviations < 15%. Fig. 13(b) focuses the comparison in the low Reynolds number region ($Re_{d_s,avg}$ < 50), where the accuracy of the state-of-the-art correlations is generally poor. In particular, the existing correlations usually underestimate the pressure drops to a different extent in this region. For instance, the correlation by Inayat et al. [19] usually predicts pressure losses 15% lower than the experimental and simulation data. Analogous results have been observed by employing the correlations by Huu et al. [20], Dietrich et al. [18] and Giani et al. [11]. Based on this work, our correlation shows a better performance in predicting the pressure drop accurately for the region of$Re_{d_s,avg}$ < 50, complementing the work by Inayat et al. [19] (which shows the good prediction of the pressure drop of foam at$Re_{d_s,avg}$ > 50). This is particularly important because the tradeoff between the pressure drop and mass transfer for foams is expected to be more favorable than that of honeycombs in the region of$Re_{d_s,avg}$ < 50.

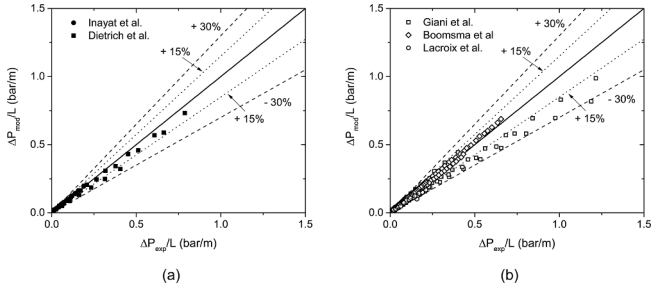

Fig. 14. Parity plot comparing the experimental and theoretical (by Eq. (12)) pressure drop for foams (a) with circular strut [39,42] and (b) triangular strut [11,15,22].

In order to further validate the proposed pressure drop correlation, the comparison is extended to experimental data with foams having circular and triangular struts, which also cover a wide range of porosity (0.74–0.95) and cell size (0.625–6.9 mm), as well as difference in working fluids and measuring conditions [11,15,22,39,42].

Fig. 14 shows the parity plot comparing the available experimental data [11,15,22,39,42] against the theoretical pressure drop predicted by the proposed correlations. In general, a good agreement between the experimental and theoretical data is confirmed under the flow rate studied with deviations of ± 15%, especially for foams with circular struts, whose constants were extracted on the basis of a large amount of data generated by this work. A slight underestimation by the correlation is found for some foams with triangular struts at relatively high flow rates [11], as shown in Fig. 14b, where the correlation underpredicts the pressure drop values at most by 30%. This can be also ascribed to the very high porosity of these foams whose struts cross-sectional shape can be even triangular concave with sharp edges leading to increased pressure drops [19].

3.6. Tradeoff between mass transfer and pressure drop in foams

Open-cell foams are considered promising for catalytic processes

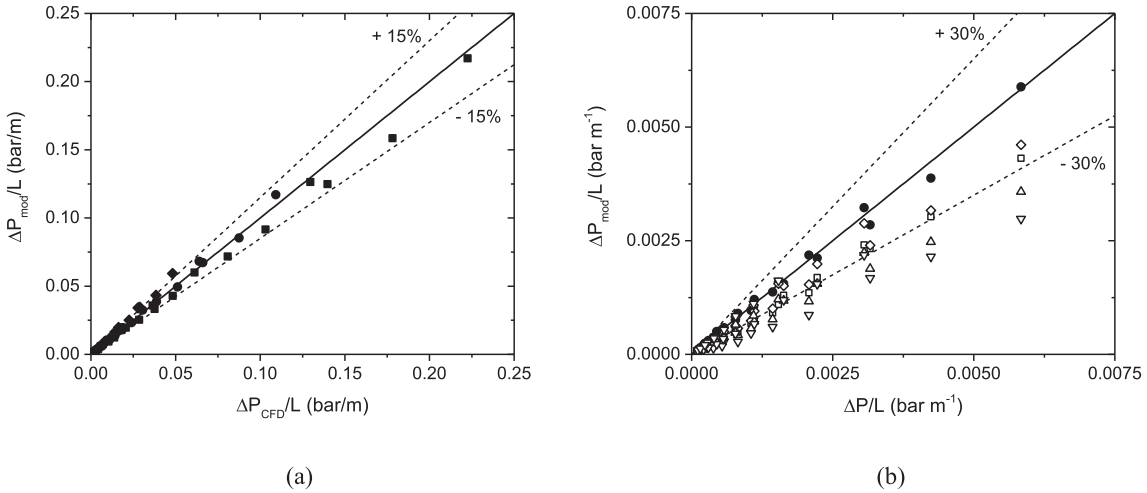

Fig. 13. Parity plot comparing the pressure drops from CFD simulations and experiments with the model predictions (a) and detailed comparison of the data by this work (full symbols) against the literature data (Inayat et al. [19] – empty square, Dietrich et al. [18] – empty diamond, Huu et al. [20] – empty upward triangle, Giani et al. [11] – downward triangle) at $\boldsymbol{Re_{d_s,avg}}$ < 50 (b).

limited by external mass transfer, such as in emission control systems for automotive and environmental applications. For emission control, reactors should usually comply with very severe constraints on the pressure drop since the engine performances are strongly affected by the pressure gradient in the exhaust system. In this regard, although the external mass transfer rate can be improved by open-cell foam, their relatively high pressure drop with respect to conventional honeycombs may hinder their adoption as the commercial solution. Thus, the mass transport and pressure drop properties of structured supports (*e.g.* honeycomb monoliths and open-cell foams) have to be assessed together for their specific target applications. In this view, Giani et al. [11] proposed a dimensionless merit index, as in Eq. (15), which ratios the mass transport to the pressure loss to quantify the tradeoff between these two pivotal properties.

$$M.\,I. = \frac{-\ln(1-\chi)}{\Delta P/(\rho u^2)} \tag{15}$$

where χ is the reactant conversion in the mass-transfer limited reactor evaluated using the mass transfer coefficient estimated with the correlation proposed in [40].

The merit index compares the external mass transfer properties in terms of conversion with the dimensionless pressure drop. Thus, the higher is the index, the better are the performances of the support. From the preliminary analysis [11], the low Reynolds number region is where the performances of open-cell foams are more promising than monoliths due to the quadratic increase of the pressure drop in foams with the velocity, which penalizes their merit index at high flow rates. Therefore, the proposed pressure drop correlation in the low Reynolds region is of great importance covering the most favorable conditions for the catalytic applications of open-cell foams.

Based on the pressure drop correlation proposed in this work and on the mass transfer correlation by Bracconi et al. [40], we compare the merit index of open-cell foams with honeycomb monoliths, as shown in Fig. 15. In this comparison, typical conditions of an after-treatment device were used for the evaluation of the relevant transport properties simulating the CO combustion in air at 573 K and 1 bar. Classical literature expressions have been adopted for honeycomb monoliths with square cells [43] without accounting for the inlet effects for both pressure drop and mass transfer. The merit index of square-celled monoliths assumes constant values which depend only on the porosity. Conversely, the merit index of foams shows a maximum over the region of Re studied. The position and the value of the maximum depends on the porosity of the foam considered. The maximum assumes lower values and moves to higher Reynolds number on decreasing the porosity. The performance of open-cell foams with circular struts can overcome that of honeycomb monoliths by *ca.* 15%, in the range of $1 \leq Re_{d_s,avg} \leq 10$, if the high porosity (*i.e.* $\varepsilon \approx 0.95$) can be applied to open-cell foams. This suggests that, in order to efficiently employ foams (with circular struts) as catalyst supports, the foam reactor should be operated within windows with low Reynolds numbers, where the tradeoff is maximum. For foams with triangular struts, clearly, the relatively high pressure drops (which cannot be compensated by the improved mass transfer rate) jeopardize the merit index, leading to the more unsatisfactory performance than monoliths.

4. Conclusions

We have performed a comprehensive analysis of pressure drops in open-cell foams using a combined numerical (CFD)/experimental method, which is based on virtual reconstruction and additive manufacturing. We demonstrated that this approach rules out all geometrical uncertainties between CAD and real models, leading to a very good agreement between the simulation and experimental data.

The systematic investigation of fluid flow in open-cell foams is carried out, revealing the effect of the geometrical properties such as cell size, porosity and strut shape on the pressure drop and leading to a deeper understanding of the interaction between the fluid flow and the structure. An increase of either the cell diameter or the void fraction reduces the pressure losses across the supports. Moreover, it is found that the average strut size is the key parameter affecting the pressure drop of gas flow through foams, as it enables to account for the effects of porosity and cell size.

Based on these findings, we proposed and validated a specific engineering Ergun-like correlation with the consideration of the cross-sectional shape of foam struts, which has shown a satisfactory agreement with the data from this work and from the literature (with deviations usually below < 15%). Two distinct sets of coefficients are proposed. Values equal to 92 and 0.71 are found for the viscous and inertial constants for circular struts. On the other hand, triangular struts require a viscous and inertial coefficient equal to 266 and 1.20, respectively. The proposed correlation enabled the accurate evaluation of the tradeoff between the external mass transfer and pressure loss, showing that open-cell foams (with circular struts) can advantageously replace the conventional honeycomb monoliths in continuous-flow catalytic applications with Re < 20.

Most importantly, this work has demonstrated the new concept of combining virtual reconstruction with additive manufacturing to effectively (*i*) close the gap between theoretical models and real structures, and (*ii*) promote the numerical/experimental investigation of structured engineering materials in view of their rational design and application.

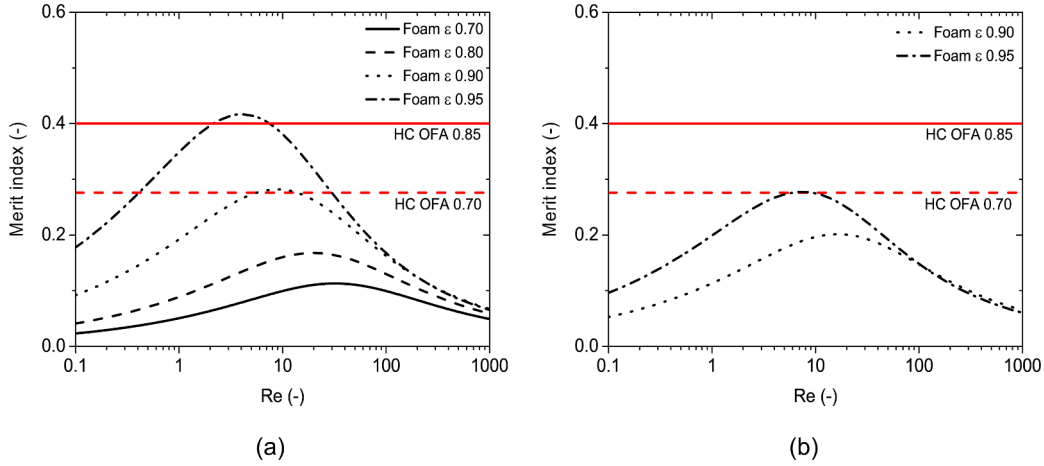

Fig. 15. Comparison of merit index for (a) foams with circular struts and (b) foams with triangular struts.

Acknowledgments

The authors acknowledge financial support from the European Research Council under the European Union's Horizon 2020 research and innovation programme (Project INTENT – Grant No. 694910). XF thanks the financial support from the Engineering and Physical Sciences Research Council (EP/R000670/1) for his research in foam materials. Computational time at CINECA (Bologna) is gratefully acknowledged. The authors of Politecnico di Milano acknowledge Ing. Valerio Mussi – MUSP – for the help in designing and manufacturing the tubular reactor.

References

[1] N. Gargiulo, D. Caputo, G. Totarella, L. Lisi, S. Cimino, Me-ZSM-5 monolith foams for the NH3-SCR of NO, Catal. Today 304 (2018) 112–118, https://doi.org/10.1016/j.cattod.2017.10.024.
[2] A. Donazzi, M. Maestri, B.C. Michael, A. Beretta, P. Forzatti, G. Groppi, E. Tronconi, L.D. Schmidt, D.G. Vlachos, Microkinetic modeling of spatially resolved autothermal CH4 catalytic partial oxidation experiments over Rh-coated foams, J. Catal. 275 (2010) 270–279, https://doi.org/10.1016/j.jcat.2010.08.007.
[3] E. Verlato, S. Barison, S. Cimino, F. Dergal, L. Lisi, G. Mancino, M. Musiani, L. Vàzquez-Gòmez, Catalytic partial oxidation of methane over nanosized Rh supported on Fecralloy foams, Int. J. Hydrogen Energy 39 (2014) 11473–11485, https://doi.org/10.1016/j.ijhydene.2014.05.076.
[4] P.H. Ho, M. Ambrosetti, G. Groppi, E. Tronconi, J. Jaroszewicz, F. Ospitali, E. Rodriguez-Castellon, G. Fornasari, A. Vaccari, P. Benito, One-step electrodeposition of Pd-CeO2 on high pore density foams for environmental catalytic processes, Catal. Sci. Technol. (2018) 4678–4689, https://doi.org/10.1039/C8CY01388H.
[5] S. Cimino, A. Gambirasi, L. Lisi, G. Mancino, M. Musiani, L. Vázquez-gómez, E. Verlato, Catalytic combustion of methanol on Pt – Fecralloy foams prepared by electrodeposition, Chem. Eng. J. 285 (2016) 276–285, https://doi.org/10.1016/j.cej.2015.09.099.
[6] Y. Jiao, S. Xu, C. Jiang, M. Perdjon, X. Fan, J. Zhang, MFI zeolite coating with intrazeolitic aluminum (acidic) gradient supported on SiC foams to improve the methanol-to-propylene (MTP) reaction, Appl. Catal. A Gen. 559 (2018) 1–9, https://doi.org/10.1016/j.apcata.2018.04.006.
[7] Y. Jiao, X. Fan, M. Perdjon, Z. Yang, J. Zhang, Vapor-phase transport (VPT) modification of ZSM-5/SiC foam catalyst using TPAOH vapor to improve the methanol-to-propylene (MTP) reaction, Appl. Catal. A Gen. 545 (2017) 104–112, https://doi.org/10.1016/j.apcata.2017.07.036.
[8] Y. Jiao, X. Yang, C. Jiang, C. Tian, Z. Yang, J. Zhang, Hierarchical ZSM-5/SiC nanowhisker/SiC foam composites: preparation and application in MTP reactions, J. Catal. 332 (2015) 70–76, https://doi.org/10.1016/j.jcat.2015.09.002.
[9] P. Yan, X. Li, H. Li, X. Gao, Hydrodynamics and flow mechanism of foam column trays: contact angle effect, Chem. Eng. Sci. 176 (2018) 220–232, https://doi.org/10.1016/j.ces.2017.10.023.
[10] X. Ou, F. Pilitsis, N. Xu, S.F.R. Taylor, J. Warren, A. Garforth, J. Zhang, C. Hardacre, Y. Jiao, X. Fan, On developing ferrisilicate catalysts supported on silicon carbide (SiC) foam catalysts for continuous catalytic wet peroxide oxidation (CWPO) reactions, Catal. Today (2018), https://doi.org/10.1016/j.cattod.2018.06.033.
[11] L. Giani, G. Groppi, E. Tronconi, Mass-transfer characterization of metallic foams as supports for structured catalysts, Ind. Eng. Chem. Res. 44 (2005) 4993–5002, https://doi.org/10.1021/ie0490886.
[12] A. Gancarczyk, M. Piątek, M. Iwaniszyn, P. Jodłowski, J. Łojewska, J. Kowalska, A. Kołodziej, In search of governing gas flow mechanism through metal solid foams, Catalysts 7 (2017) 124, https://doi.org/10.3390/catal7040124.
[13] J. Richardson, Y. Peng, D. Remue, Properties of ceramic foam catalyst supports: pressure drop, Appl. Catal. A Gen. 204 (2000) 19–32, https://doi.org/10.1016/S0926-860X(00)00508-1.
[14] G. Incera Garrido, F.C. Patcas, S. Lang, B. Kraushaar-Czarnetzki, Mass transfer and pressure drop in ceramic foams: a description for different pore sizes and porosities, Chem. Eng. Sci. 63 (2008) 5202–5217, https://doi.org/10.1016/j.ces.2008.06.015.
[15] M. Lacroix, P. Nguyen, D. Schweich, C. Pham Huu, S. Savin-Poncet, D. Edouard, Pressure drop measurements and modeling on SiC foams, Chem. Eng. Sci. 62 (2007) 3259–3267, https://doi.org/10.1016/j.ces.2007.03.027.
[16] D. Edouard, M. Lacroix, C.P. Huu, F. Luck, Pressure drop modeling on SOLID foam: state-of-the art correlation, Chem. Eng. J. 144 (2008) 299–311, https://doi.org/10.1016/j.cej.2008.06.007.
[17] J. Ahmed, C. Pham-Huu, D. Edouard, A predictive model based on tortuosity for pressure drop estimation in "slim" and "fat" foams, Chem. Eng. Sci. 66 (2011) 4771–4779, https://doi.org/10.1016/j.ces.2011.06.040.
[18] B. Dietrich, Pressure drop correlation for ceramic and metal sponges, Chem. Eng. Sci. 74 (2012) 192–199, https://doi.org/10.1016/j.ces.2012.02.047.
[19] A. Inayat, M. Klumpp, M. Lämmermann, H. Freund, W. Schwieger, Development of a new pressure drop correlation for open-cell foams based completely on theoretical grounds: Taking into account strut shape and geometric tortuosity, Chem. Eng. J. 287 (2016) 704–719, https://doi.org/10.1016/j.cej.2015.11.050.
[20] T.T. Huu, M. Lacroix, C. Pham Huu, D. Schweich, D. Edouard, Towards a more realistic modeling of solid foam: use of the pentagonal dodecahedron geometry, Chem. Eng. Sci. 64 (2009) 5131–5142, https://doi.org/10.1016/j.ces.2009.08.028.
[21] K. Boomsma, D. Poulikakos, Y. Ventikos, Simulations of flow through open cell metal foams using an idealized periodic cell structure, Int. J. Heat Fluid Flow 24 (2003) 825–834, https://doi.org/10.1016/j.ijheatfluidflow.2003.08.002.
[22] K. Boomsma, D. Poulikakos, The effects of compression and pore size variations on the liquid flow characteristics in metal foams, J. Fluids Eng. 124 (2002) 263, https://doi.org/10.1115/1.1429637.
[23] X. Fan, X. Ou, F. Xing, G.A. Turley, P. Denissenko, M.A. Williams, N. Batail, C. Pham, A.A. Lapkin, Microtomography-based numerical simulations of heat transfer and fluid flow through β-SiC open-cell foams for catalysis, Catal. Today 278 (2016) 350–360, https://doi.org/10.1016/j.cattod.2015.12.012.
[24] Z. Nie, Y. Lin, Q. Tong, Numerical investigation of pressure drop and heat transfer through open cell foams with 3D Laguerre-Voronoi model, Int. J. Heat Mass Transfer 113 (2017) 819–839, https://doi.org/10.1016/j.ijheatmasstransfer.2017.05.119.
[25] M. Bracconi, M. Ambrosetti, M. Maestri, G. Groppi, E. Tronconi, A systematic procedure for the virtual reconstruction of open-cell foams, Chem. Eng. J. 315 (2017) 608–620, https://doi.org/10.1016/j.cej.2017.01.069.
[26] P. Habisreuther, N. Djordjevic, N. Zarzalis, Statistical distribution of residence time and tortuosity of flow through open-cell foams, Chem. Eng. Sci. 64 (2009) 4943–4954, https://doi.org/10.1016/j.ces.2009.07.033.
[27] P. Kumar, F. Topin, State-of-the-art of pressure drop in open-cell porous foams: review of experiments and correlations, J. Fluids Eng. 139 (2017) 111401, , https://doi.org/10.1115/1.4037034.
[28] L.J. Gibson, M.F. Ashby, Cellular Solids: Structure and Properties, Cambridge University Press, 1999.
[29] M. Ambrosetti, M. Bracconi, G. Groppi, E. Tronconi, Analytical geometrical model of open cell foams with detailed description of strut-node intersection, Chem.-Ing.-Tech. 89 (2017) 915–925, https://doi.org/10.1002/cite.201600173.
[30] H. Jasak, A. Jemcov, Z. Tukovic, OpenFOAM: a C + + library for complex physics simulations, Int. Work. Coupled Methods Numer. Dyn. (2007) 1–20.
[31] S. Razza, T. Heidig, E. Bianchi, G. Groppi, W. Schwieger, E. Tronconi, H. Freund, Heat transfer performance of structured catalytic reactors packed with metal foam supports: Influence of wall coupling, Catal. Today 273 (2016) 187–195, https://doi.org/10.1016/j.cattod.2016.02.058.
[32] A. Della Torre, G. Montenegro, G.R. Tabor, M.L. Wears, CFD characterization of flow regimes inside open cell foam substrates, Int. J. Heat Fluid Flow 50 (2014) 72–82, https://doi.org/10.1016/j.ijheatfluidflow.2014.05.005.
[33] F.P.W. Melchels, J. Feijen, D.W. Grijpma, A review on stereolithography and its applications in biomedical engineering, Biomaterials 31 (2010) 6121–6130, https://doi.org/10.1016/j.biomaterials.2010.04.050.
[34] E. Bianchi, T. Heidig, C.G. Visconti, G. Groppi, H. Freund, E. Tronconi, An appraisal of the heat transfer properties of metallic open-cell foams for strongly exo-/endothermic catalytic processes in tubular reactors, Chem. Eng. J. 198–199 (2012) 512–528, https://doi.org/10.1016/j.cej.2012.05.045.
[35] S. Ergun, A.A. Orning, Fluid flow through randomly packed columns and fluidized beds, Ind. Eng. Chem. 41 (1949) 1179–1184, https://doi.org/10.1021/ie50474a011.
[36] J. Kozeny, Uber kapillare Leitung des Wassers im Boden (Aufstieg, Versickerung und Andwendung auf die Bewasserung), Sber. Akad. W&-s, Wien, 1927.
[37] I.F. Macdonald, M.S. El-Sayed, K. Mow, F.A.L. Dullien, Flow through porous media-the ergun equation revisited, Ind. Eng. Chem.Fundam. 18 (1979) 199–208, https://doi.org/10.1021/i160071a001.
[38] O. Al-Ketan, R. Rowshan, R.K. Abu Al-Rub, Topology-mechanical property relationship of 3D printed strut, skeletal, and sheet based periodic metallic cellular materials, Addit. Manuf. 19 (2018) 167–183, https://doi.org/10.1016/j.addma.2017.12.006.
[39] B. Dietrich, W. Schabel, M. Kind, H. Martin, Pressure drop measurements of ceramic sponges-determining the hydraulic diameter, Chem. Eng. Sci. 64 (2009) 3633–3640, https://doi.org/10.1016/j.ces.2009.05.005.
[40] M. Bracconi, M. Ambrosetti, M. Maestri, G. Groppi, E. Tronconi, A fundamental investigation of gas/solid mass transfer in open-cell foams using a combined experimental and CFD approach, Chem. Eng. J. 352 (2018) 558–571, https://doi.org/10.1016/j.cej.2018.07.023.
[41] S. Ergun, Fluid flow through packed columns, Chem. Eng. Prog. 48 (1952) 89–94 doi:citeulike-article-id:7797897.
[42] A. Inayat, H. Freund, A. Schwab, T. Zeiser, W. Schwieger, Predicting the specific surface area and pressure drop of reticulated ceramic foams used as catalyst support, Adv. Eng. Mater. 13 (2011) 990–995, https://doi.org/10.1002/adem.201100038.
[43] R.K. Shah, A.L. London, Laminar Flow Forced Convection in Ducts: A Source Book for Compact Heat Exchanger Analytical Data, Academic press, 1978.